Contract No.:

This manuscript has been authored by Savannah River Nuclear Solutions (SRNS), LLC under Contract No. DE-AC09-08SR22470 with the U.S. Department of Energy (DOE) Office of Environmental Management (EM).

Disclaimer:

The United States Government retains and the publisher, by accepting this article for publication, acknowledges that the United States Government retains a non-exclusive, paid-up, irrevocable, worldwide license to publish or reproduce the published form of this work, or allow others to do so, for United States Government purposes.

Nepheline Crystallization and the Residual Glass Composition: Understanding Waste Glass Durability

Devon L. McClane[1,*], Jake W. Amoroso[1], Kevin M. Fox[1], Madison C. Hsieh[1], Matthew R. Kesterson[1], Albert A. Kruger[2]

[1]Savannah River National Laboratory, 227 Gateway Dr., 999-W, Aiken, SC 29803, USA
[2]U.S. Department of Energy, Office of River Protection, P.O. Box 450, MSIN H6-60, Richland, WA 99352, USA

[*]Corresponding Author E-mail address: Devon.Mcclane@srnl.doe.gov

Abstract

The vast majority of High-Level Waste (HLW) originating from defense nuclear programs is sequestered and immobilized in borosilicate glass. Borosilicate glass is universally accepted for immobilizing HLW, but its efficiency has limitations based on the compositional makeup of the waste stream. The chemical durability of the glass is the most important factor in determining the longevity and usefulness of the final glass waste form. The primary detriment to this durability in glasses containing high levels of aluminum is nepheline ($NaAlSiO_4$) crystallization, as it is generally accompanied by a measurable decrease in the glass's chemical durability. This work seeks to understand nepheline crystallization, within the context of thermal history, and to elucidate the influence of compositional shifts in the residual glass (after crystallization) on the measured durability. The results presented within show a distinct deviation in leaching behavior as a function of structural makeup (calculated Q units). This understanding will provide practical information required for broadening glass compositional regions needed to more efficiently vitrify HLW.

1 Introduction

The United States Department of Energy (DOE) Office of River Protection (ORP) plans to process the bulk of the 56 million gallons of radioactive waste, stored in the Tank Farms at the Hanford Site, through the Waste Treatment and Immobilization Plant (WTP)(1). This waste, which will be separated into Low-Activity Waste (LAW) and High-Level Waste (HLW) streams, will ultimately be vitrified in borosilicate glasses poured into stainless steel canisters. While the waste loading in LAW glasses is typically limited by the solubility limits of select waste stream components (such as sulfur) in the glass melt(2), the waste loading in HLW glasses is typically restricted by compositional constraints imposed during processing to avoid undesirable crystallization in the melter and canister during cooling(3). For example, the utilization of a Nepheline Discriminator (ND)(4, 5), shown in Equation 1, restricts the ratio amongst Al_2O_3, Na_2O, and SiO_2 in the glass to relatively high values of SiO_2 (greater than or equal to 62 wt%).

$$ND = \frac{SiO_2}{Al_2O_3 + Na_2O + SiO_2} \geq 0.62 \qquad (1)$$

Although this processing constraint has been successfully used to ensure HLW glasses processed through the Defense Waste Processing Facility (DWPF) display comparatively low leaching (i.e., high chemical durability), it may also unnecessarily restrict waste loading, contributing to excessive life-cycle duration and associated costs. While targeted waste loadings at DWPF are around 36 wt%[6] and are generally limited by other constraints (e.g. liquidus temperature, viscosity, etc.)[7], the HLW at Hanford contains significantly higher concentrations of Al_2O_3[8] which limits the projected waste loading of a large portion of the glass processed through WTP to ~18 wt% if the ND constraint is applied[3, 9]. Because of this reality, much research in the last decade has focused on understanding factors that contribute to nepheline ($NaAlSiO_4$) formation in waste glasses containing relatively high levels of sodium and aluminum, in an attempt to find composition regions that are resilient to nepheline formation without adhering to the current ND[9-12]. Despite these efforts; the complexity of the HLW glass compositions combined with known changes in glass durability with crystallization[13], and additional constraints required to ensure glass processability, have precluded identification of an optimized glass composition region. In this work, we seek to understand crystallization in waste glass formulations, under the context of its thermal history, by utilizing thermal models simulating glass cooling at various radial locations within a canister after pouring. The results of this approach illustrate realistic performance of waste glass as a function of crystallization behavior and relative nepheline concentration in a full-scale canister. In addition, this research seeks to demonstrate the importance of understanding nucleation behavior (surface vs. bulk) and how the residual glass composition impacts the performance of the final waste form, adding further variables for consideration when developing future glass composition regions.

2 Experimental Procedures

2.1 Glass Composition Selection and Processing

Three glass compositions were chosen to investigate the influence of cooling rate on observed nepheline crystallization and subsequent durability. Table 1 lists the component oxide composition of the three glasses designated NP2-23, NP-MC-BNa-1, and NP2-23_High Al. Two of the study glasses, NP2-23 and NP-MC-BNa-1, were previously studied and exhibited a predominance for surface or bulk crystallization, respectively[10, 14, 15]. The third glass composition, NP2-23_High Al, was selected, by substituting 4.78 wt% Al_2O_3 for Fe_2O_3 in NP2-23. This was intended to investigate whether a higher alumina loading could be achieved in a glass displaying crystallization only on the surface.

Batches were prepared by manually mixing stochiometric amounts of reagent grade oxides, carbonates, sulfates, phosphates, boric acid, sodium fluoride, and ruthenium chloride. These batches were then heated from ambient temperature to 1200°C in covered Pt-10Rh crucibles, isothermally held for approximately one hour, and water-quenched. To ensure homogeneity, the resulting glass was ground using an Angstrom TE250 Ring Pulverizer with tungsten carbide grinding container (Angstrom, Inc., Belleville, MI), re-melted at 1200°C for one hour, and water-quenched. This glass was re-ground and used as feed material for subsequent testing.

A sample of each quenched and ground glass was prepared for chemical analysis utilizing lithium metaborate and sodium peroxide/sodium hydroxide fusions. Chemical analysis on the suite of constituent cations in each glass was performed using an Agilent 730 ES Simultaneous Inductively Coupled Plasma – Atomic Emission Spectrometer (ICP-AES) (Agilent Technologies, Santa Clara, CA). Table 1 summarizes targeted and measured compositions of the study glasses, of which the differences were considered acceptable, as well as the theoretical maximum nepheline concentrations calculated from Na_2O, Al_2O_3, and SiO_2 contents. The limiting oxide for nepheline formation is bolded in Table 1.

2.2 Heat Treatment

Crystallization in glasses is a dynamic process that can involve complex heterogeneous and homogeneous nucleation and crystallization phenomena that can result in either bulk or surface crystallization depending on the presence of pre-existing nucleation sites and kinetic factors for crystal growth such as temperature, activation energy and rate of diffusion[16-21]. If these processes are unknown or not fully understood, then conclusions drawn from laboratory-scale testing may be unsuitable, or even misleading, when applied to full-scale operations. The primary reason for this discrepancy is a lack of scalability. In full-scale operation, several hundred kilograms of glass are processed (melted, poured into a canister, and cooled via natural radiation and convection) over the course of >24 hours, which creates thermal gradients in excess of 500°C throughout the canister, as shown in Figure 1. In particular, the surface of the canister is much colder than the interior and has been simulated to reach a maximum temperature of ~400°C[22]. This temperature is assumed to be sufficiently low enough to prevent crystallization. While this observation has little impact on glasses that exhibit bulk crystallization, it is important for modeling the impact of surface crystallization. In other words, if no substantial nucleation sites exist within the glass, and the surface temperature is not high enough to allow for crystal growth, no crystallization would be expected. Because of this,

great care was taken to heat treat glasses in this study such that they experienced a known thermal history that could be correlated back to specific areas within a canister.

Cooling profiles were derived by mapping the anticipated glass temperatures, within a WTP canister, using output from a COMSOL® Multiphysics model. A representative set of simulated temperatures was extracted from six locations distributed at radial distances of 0.0, 15.24, 22.86, 26.67, 28.575, and 30.48 centimeters from the centerline of the canister and at the approximate midpoint height of 2.44 meters(22). These locations are shown graphically in Figure 1. An additional cooling profile, referred to as canister centerline cooling (CCC), typically used to study nepheline crystallization and described elsewhere(15) was also included in this study for comparison. All glass compositions were heat treated using a Thermolyne 48000 furnace (Thermo Fisher Scientific, Waltham, MA). Approximately 30 grams of each glass were heat treated in covered 30 mL Pt-5Au crucibles. In addition, approximately 2 grams of NP2-23, a glass known to exhibit pronounced surface crystallization, were heat treated in covered 2 cm^3 Pt-5Au cubic pans to accentuate the influence of relative surface area on laboratory results. The glasses were melted at 1200°C for approximately one hour, and immediately heat treated according to the cooling programs shown in Table 2. Some cooling profiles required an initial temperature decrease faster than what could be achieved in a single furnace. In these instances, the glass was moved from the melting furnace to a pre-heated secondary furnace and allowed to dwell for 15 minutes prior to initiating the program. Glasses were removed from the heat treatment furnace once the temperature was below 100°C, well below any temperature anticipated to influence measured results.

2.3 Microscopy

Optical microscopy was used to image crystal development after heat treatment. A thin section (< 1mm) was cut from the middle of select heat treated samples using a Buehler Isomet™ low speed saw (Buehler, Lake Bluff, IL) and subsequently polished using an Allied Multiprep™ precision polishing system (Allied High-Tech Products, Inc., Rancho Dominguez, CA). An Olympus SZX16 optical microscope equipped with Olympus UC50 camera (Olympus Corporation, Center Valley, PA) was used to record optical images. Scanning electron microscopy (SEM), performed with a Hitachi TM3000 tabletop SEM equipped with energy dispersive spectroscopy (EDS) (Hitachi TM3000, Japan) was used to investigate chemical distribution, identification, and morphology of crystalline phases after heat treatment.

2.4 Durability

Each heat-treated specimen, described in Section 2.2, was ground in its entirety for durability measurement. Durability was performed in accordance with Method A of ASTM C1285 (the Product Consistency Test, or PCT)(23)

on 1.5 gram samples of the ground glass. Normalized release of specific elements was calculated according to Equation 2, where R_i is the fractional release (%) of element i, C_i is the concentration of element i measured in the leachate (g/L), V is the volume of leachate used in the PCT (L), f_i is the targeted mass fraction of element i in the un-leached glass, and M is the mass of sample used in the PCT (g). Normalized release was also calculated for residual glass compositions corrected for measured crystallinity, determined from quantitative XRD analyses, by assuming the crystalline phases did not leach.

$$R_i = \frac{C_i V}{f_i M_i} \times 100\%$$ (2)

2.5 Phase Analysis

Powder X-ray diffraction (PXRD) was used to identify crystal phases in heat treated glasses. -200 mesh powders from preparation of glass durability measurement were mixed with a calcium fluoride standard for quantitative PXRD measurement. PXRD spectra were collected from 5 – 70° 2θ using a Bruker D8 X-ray Diffractometer (Bruker AXS Inc., Madison, WI) with Cu Kα source, 0.02° step size, and 1 s/step scan rate. Crystal phase identification, and relative concentration, were analyzed via Jade™ software (Version 2010) from Materials Data Inc., with the PDF-4 database from the International Centre for Diffraction Data.

3 Results and Discussion

Cooling profiles designed to mimic cooling rates experienced in a canister during processing, and discussed in Section 2.2, were recorded during each furnace heat treatment (HT) and are shown in Figure 2. The maximum recorded temperature, as well as time spent in the nepheline crystallization temperature regime (assumed to be between 500°C and 900°C based on previous research[10]), decreases towards the canister wall and away from the centerline, as expected, with times ranging from 21.5 hours for CCC HT to 0.0 hours for 30.48 HT.

3.1 Characterization of Crystalline Phases and Residual Glass

Thin cross sections cut from select glass samples were examined to provide insight on how the glasses crystallized during slow cooling. Figure 3 shows representative optical images and SEM-EDS chemical mapping for each glass composition after heat treatment. NP2-23 and NP2-23_High Al primarily crystallized at the crucible interface, whereas NP-MC-BNa-1 crystallized throughout the glass. SEM/EDS analysis performed on glass near the crucible interface of the NP2-23 sample revealed a phase rich in Al (as well as Na and Si, indicative of nepheline) and another phase rich in Ca (as well as several other elements added during batching, indicative of the residual glass). Similar devitrification, albeit different in morphology and thickness, was observed in the NP2-23_High Al glass near

the crucible interface. SEM/EDS analysis performed near the center of the NP-MC-BNa-1 sample confirmed a distinct nepheline phase, residual glassy phase, and a third phase rich in Fe, Cr, and Mn presumed to be spinel. The nepheline phase appeared lighter in backscattered electron imaging than the residual glass in NP-MC-BNa-1, but darker than the residual glass in both NP2-23 and NP2-23_High Al. Since the average atomic number for $NaAlSiO_4$ (10) was higher than values calculated for all glasses, and therefore should have appeared brighter, this may indicate that Li is partially substituting for Na in the nepheline crystalline phase in these glasses, a phenomena observed elsewhere[24, 25].

Quantitative XRD results are shown in Table 3. These results, normalized to maximum theoretical nepheline concentration to show relative propensity for crystallization, are shown in Figure 4. An expected increase in nepheline concentration is generally observed with heat treatment corresponding to location moving towards the center of the canister. The differences between NP2-23_Cruc and NP2-23_Pan (an approximate 2x increase in crystallization compared to ~3x increase in specific bulk surface area) are used to highlight potential differences between laboratory scale and full-scale (an anticipated ~100x decrease in specific bulk surface area compared to NP2-23_Pan). In addition, the observed increase in crystallization in NP2-23_High Al compared to NP2-23 provides insight as to how the residual glass matrix may alter the rate of diffusion for crystal growth. The only difference between these glasses was a substitution of 4.72 wt.% Al_2O_3 for Fe_2O_3, in NP2-23_High Al. This compositional adjustment effectively removed a glass modifier and replaced it with a diffusing species required for nepheline formation, resulting in a substantial increase in observed nepheline crystallization (increase from 3.9 to 38.4 wt% for CCC specimens).

To further investigate this compositional influence, quantitative phase analysis was used to calculate a residual glass composition (f_{i_g}) for each sample according to Equation 3, the results of which will be referred to throughout subsequent discussion. In Equation 3, f_i is the mass fraction of element i in the targeted glass composition, N_i is the mass fraction of element i in nepheline, and X is the concentration of nepheline (mass fraction). A residual glass composition was also calculated for crystalline concentrations up to the maximum theoretical nepheline concentration given in Table 1.

$$f_{i_g} = \frac{f_i - XN_i}{(1-X)} \tag{3}$$

Based on the residual glass composition, non-bridging oxygen (NBO) and coordination units (Q units) can be estimated, providing structural insight. Specifically, Q units provide information on the structural coordination of the tetrahedron, while NBO ratios relative to SiO_2, have been suggested to be an indicator as to the rate of diffusion in glass, with higher NBO values corresponding to lower viscosities[26, 27] and therefore faster rates of diffusion[28].

NBO were calculated according to the equation proposed by McClane et. al[10], shown in Equation 4, the results of which are included in Table 3. Calculated NBO were subsequently used to calculate Q units, shown in Figure 5, based on their respective relation discussed by Shelby[29]. This analysis shows that both residual glasses of NP2-23 and NP2-23_High Al maintained tetrahedron coordination consisting of Q^3 and Q^2 (NBO between 1 and 2) for all crystallization observed under conditions mimicking canister cooling. In comparison, the residual glass composition of NP-MC-BNa-1, loses structural integrity as the composition shifts from a glassy silicate material to an alkali alumina-borate phase. This change is directly attributed to nepheline crystallization since SiO_2 is the limiting constituent for its growth.

$$NBO = \frac{2(Li_2O + Na_2O + MgO + CaO + MnO + NiO + Fe_2O_3 - Al_2O_3) + B_2O_3 + TiO_2 - ZrO_2}{SiO_2} \tag{4}$$

3.2 Chemical Durability

Chemical durability, as measured by elemental release from the PCT, was normalized to the targeted glass compositions according to Equation 2, as well as to the residual glass composition, calculated according to Equation 5, where R_{i_g} is the fractional release (%) of element i leached from the glass, C_i is the concentration of element i measured in the leachate (g/L), V is the volume of leachate used in the PCT (L), f_{i_g} is the mass fraction of element i in the residual glass, M is the mass of sample used in the PCT (g), and X is the concentration of nepheline (mass fraction) determined from quantitative XRD analysis.

$$R_{i_g} = \frac{C_i V}{f_{i_g} M (1-X)} \times 100\% \tag{5}$$

Normalized elemental release was less than 2% for any single component in glasses exhibiting surface crystallization (NP2-23 & NP2-23_High Al). While there was a general increase in elemental release with increasing nepheline concentration for those glasses, the magnitude difference in elemental release was comparable for glasses containing up to 40 wt% nepheline. The observed increase in leaching is consistent with calculated changes in the glass structure, with NP2-23_High Al displaying higher durability than NP2-23 at low crystallization concentrations. This comparatively higher durability is removed with longer heat treatment due to the higher propensity for crystallization observed in NP2-23_High Al. In addition, the observed non-linear increase in Al_2O_3 leaching from the residual glass for NP2-23_High Al with increasing nepheline concentration matches a change in the structural role of Al in the glass reported by Vienna et al.[30].

The glass with bulk crystallization (NP-MC-BNa-1) exhibited significantly higher normalized elemental release, which generally increased with increasing nepheline content. This glass also displayed three distinctly different leaching behaviors depending on the quantified nepheline concentration (a function of HT). With relatively low crystallinity (0-2.2 wt% NaAlSiO$_4$, corresponding to Q3 and Q2 structural units) congruent leaching among elements is observed, exhibiting normalized elemental release values less than 10%. When nepheline was present at 37 wt% (corresponding to Q2 and Q1 structural units), alkali, boron, and sulfur appear to have been preferentially leached. When nepheline is present in high concentrations >50 wt%, corresponding to a lack of tetrahedron coordination, alkali components and sulfur appear to be selectively leached (up to ~90%). In addition, no boron leaching was observed in these specimens. This apparent change in leaching behavior, specifically as it applies to boron, can be understood more clearly through compositional mapping analysis, presented subsequently.

3.3 Compositional Mapping

Kim et al(13) proposed that compositional changes to HLW glasses induced through crystallization can be used to understand the leaching behavior. In other words, the leaching behavior should be assessed with respect to the crystalline phase(s) and the residual glass composition. Therefore, in order to better understand the leach results, ternary phase diagrams originally proposed by Lambotte(31) and Abdullaev(32) were modified to include the calculated residual glass compositions, after normalizing to remove the measured nepheline concentration, presented in Figure 7. Also shown in Figure 7, is the calculated final glass composition post-leaching (f_{i_L}), calculated according to Equation 6 where f_i is the mass fraction of element i in the targeted glass composition, N_i is the mass fraction of element i in nepheline, C_i is the concentration of element i in the leachate (g/L), X is the concentration of nepheline (mass fraction), M is the mass of sample used in the PCT (g), V is the volume of leachate used in the PCT (L), and g_i is the corresponding gravimetric factor needed to convert elemental concentrations to the oxides listed in Table 1. These results show how the residual glass is altered during leaching and help demonstrate the magnitude of incongruent leaching observed.

$$f_{i_L} = \frac{M(f_i - XN_i) - C_iV}{M(1-X) - V\sum C_ig_i} \times 100\% \tag{6}$$

As shown in Figure 7a, the residual glass compositions of both NP2-23 and NP2-23_High Al shift from within the nepheline primary phase field (Ne) towards a higher SiO$_2$ region that lies above the nepheline discriminator (orange line), with increasing NaAlSiO$_4$ content. Additionally, there is a likely gradient in these glasses, since they displayed surface crystallization, with actual compositions ranging from the baseline (targeted) in the center of the

crucible, to a composition close to that calculated for residual compositions with maximum nepheline crystalized, which would lie on the respective Na_2O-SiO_2 and Na_2O-B_2O_3 binaries, at the crucible interface. In contrast, the residual glass composition of NP-MC-BNa-1 shifts from the relative center of the ternary diagrams to a comparatively high boron-high alumina region (Figure 7b and 7a, respectively), with increasing $NaAlSiO_4$.

While post-leaching compositions of NP2-23 and NP2-23_High Al lie on top of their post-crystallization counterparts (indicative of congruent leaching and why they are not distinguishable in Figure 7), NP-MC-BNa-1 shows a significant change in composition post-leaching. As seen in Figure 7b, the glass containing an intermediate crystal concentration of 37 wt% pushed the residual glass (normalized to Na_2O, Al_2O_3, and B_2O_3 concentrations) into a $NaAlB_2O_5$ phase field, which presumably lent itself to increased boron leaching (i.e., this quantity of crystallization formed a residual glass phase that was more susceptible to chemical degradation of boron). This same glass with higher nepheline crystallization, resulted in a residual glass outside of this phase field, and subsequently only leached alkali and sulfur, the results of which indicate that preferential leaching may be able to be tailored for select glass compositions, and provides further support that the extent of crystallinity and its influence on the residual glass composition has a profound effect on leaching behavior.

3.4 Practical Application

Taken together, the results lend purpose to assessing nepheline crystallization in HLW glasses using realistic thermal history and the residual glass composition. Overall, the results suggest that two different control strategies for allowing an increase in alumina waste loading while ensuring HLW glass maintains an acceptable durability upon slow-cooling may be viable. The first strategy is to control the glass composition so that nepheline preferentially crystallizes at the surface (i.e., canister wall). As shown in Table 3, all tested glasses that exhibited surface crystallization behavior showed no quantifiable crystallinity under conditions mimicking a cooling rate prototypic of contact with the canister wall and subsequently, durability was acceptable. Furthermore, any volume of crystallization that may occur at the canister wall, such as the quantities seen with other cooling profiles, would be expected to be negligible compared to the total volume of glass in an actual waste canister due to the low specific surface area (~7 m^{-1}) associated with a cylindrical canister containing ~3000 kg of glass. A second strategy would focus on controlling the glass composition so that as it experiences the time/temperature conditions associated with canister cooling, and select elements are sequestered to a crystalline phase, the residual glass maintains its chemical integrity. This strategy would benefit from mapping changes to the residual glass composition to ensure regions prone to leaching are avoided,

as well as calculating NBO and Q units to quantify structural integrity although potential inhomogeneities within the residual glass adds a further level of complication.

4 Summary

Three glasses with varying Al_2O_3 concentrations were fabricated and heat treated following cooling protocols intended to mimic conditions prototypic of varying radial distances within a WTP HLW canister. The observed crystallinity (ranging from 0 wt% for cooling profiles representative of conditions at the canister wall to 74 wt% for rates experienced in the bulk glass) displayed dependency on glass composition, heat treatment times/temperatures, and for glasses that displayed surface crystallization; specific surface area (i.e., quantity of nucleation sites). Nepheline crystallization, and its impact on waste form durability (determined via the Product Consistency Test) was attributed to the influence of crystallization on the residual glass composition. Two of the study glasses, NP2-23 and NP2-23_High Al, largely maintained their chemical durability due to the glass maintaining its structural integrity (comprised of Q3 and Q2 units) with measured elemental release values remaining under 2%. In the case of NP-MC-BNa-1, leaching results shifted from congruent leaching (when the glass was comprised of Q3 and Q2 units) to preferential leaching of alkali and boron (when the glass was comprised of Q2 and Q1 units), to almost complete leaching of only alkali and sulfur (when the residual glass was no longer silica based). These results imply that a more complete understanding of factors that influence glasses to preferentially crystallize at the surface, and/or how anticipated crystallization will alter residual glass structure and leaching behavior, offer the potential for opening glass compositional regimes needed to more efficiently vitrify HLW.

Acknowledgements

References

1.   Smith KW, Harp BJ, Fletcher TW, Hamel WF. River Protection Project System Plan. Richland, Washington: U.S. Department of Energy Office of River Protection; 2014. Contract No.: ORP-11242, Revision 7.

2.   Peeler D, Kim D-S, Vienna J, Schweiger M, Piepel G. Office of River Protection Advanced Low-Activity Waste Glass Research and Development Plan. Richland, Washington: Pacific Northwest National Laboratory; 2015. Contract No.: PNNL-24883.

3.   Vienna J, Kim D, Schweiger M, Piepel G, Kroll J, Kruger A. Glass Formulation and Testing for U.S. High-Level Tank Wastes Project 17210 Year 1 Status Report: October 15, 2014. 2014. Contract No.: PNNL-SA-84872.

4.   Li H, Vienna J, Hrma P, E. Smith D, J. Schweiger M. Nepheline Precipitation in High-Level Waste Glasses: Compositional Effects and Impact on the Waste Form Acceptability. Materials Research Society Proceedings. 1997;465:261-8.

5.   M. FK, B. ET, K. PD. Control of Nepheline Crystallization in Nuclear Waste Glass. International Journal of Applied Ceramic Technology. 2008;5(6):666-73.

6.   Pareizs J, Click D, Lambert D, Reboul S. SLUDGE BATCH 7B QUALIFICATION ACTIVITIES WITH SRS TANK FARM SLUDGE. Aiken, SC: Savannah River National Laboratory; 2011 2011-11-16. Report No.: SRNL-STI-2011-00548; TRN: US1200067 United States 10.2172/1030794 TRN: US1200067 available SRS English Contract No.: SRNL-STI-2011-00548.

7.   Edwards TB, Brown KG, Postles RL. SME Acceptability Determination for DWPF Process Control. Aiken, SC Washington Savannah River Company; 2006. Contract No.: U.S. Department of Energy Report WSRC-TR-95-00364, Revision 5.

8.   Goel A, McCloy JS, Pokorny R, Kruger AA. Challenges with vitrification of Hanford High-Level Waste (HLW) to borosilicate glass – An overview. Journal of Non-Crystalline Solids: X. 2019;4:100033.

9.   Vienna JD, Kroll JO, Hrma PR, Lang JB, Crum JV. Submixture model to predict nepheline precipitation in waste glasses. International Journal of Applied Glass Science. 2017;8(2):143-57.

10.   McClane DL, Amoroso JW, Fox KM, Kruger AA. Nepheline crystallization behavior in simulated high-level waste glasses. Journal of Non-Crystalline Solids. 2019;505:215-24.

11.   Goel A, McCloy JS, Fox KM, Leslie CJ, Riley BJ, Rodriguez CP, et al. Structural analysis of some sodium and alumina rich high-level nuclear waste glasses. Journal of Non-Crystalline Solids. 2012;358(3):674-9.

12.   Vienna JD, Skorski DC, Kim DS, Matyas J. Glass Property Models and Constraints for Estimating the Glass to be Produced at Hanford by Implementing Current Advanced Glass Formulation Efforts. Richland, Washington: Pacific Northwest National Laboratory; 2013. Contract No.: PNNL-22631, Rev. 1.

13.   Kim DS, Peeler DK, Hrma P. Effect of Crystallization in the Chemical Durability of Stimulated Nuclear Waste Glasses. In: Jain V, Palmer R, editors. CERAMIC TRANSACTIONS; Cincinnati, OH: ACS; 1995. p. 177-86.

14.   Amoroso J. The Impact of Kinetics On Nepheline Formation in Nuclear Waste Glasses. Aiken, SC: Savannah River National Laboratory; 2011. Report No.: SRNL-STI-2011-00051; TRN: US1102158 United States 10.2172/1011079 TRN: US1102158 available SRS English Contract No.: SRNL-STI-2011-00051.

15.   Kroll J, Vienna J, Schweiger MJ, Piepel G, Cooley S. Results from Phase 1, 2, and 3 Studies on Nepheline Formation in High-Level Waste Glasses Containing High Concentrations of Alumina. Richland, WA: Pacific Northwest National Laboratory; 2016. Contract No.: PNNL-26057.

16.   Müller R, Zanotto ED, Fokin VM. Surface crystallization of silicate glasses: nucleation sites and kinetics. Journal of Non-Crystalline Solids. 2000;274(1):208-31.

17.   Fokin V, Zanotto E, Yuritsyn N, Schmelzer J. Homogeneous Crystal Nucleation in Silicate Glasses: A 40 Years Perspective. Journal of Non-Crystalline Solids. 2006;352:2681-714.

18.   Deubener J. Structural aspects of volume nucleation in silicate glasses. Journal of Non-Crystalline Solids. 2005;351(18):1500-11.

19.   Kirkpatrick RJ. Crystal growth from the melt: a review. American Mineralogist: Journal of Earth and Planetary Materials. 1975;60(9-10):798-814.

20.   Schmelzer JWP, Abyzov AS, Fokin VM, Schick C, Zanotto ED. Crystallization in glass-forming liquids: Effects of fragility and glass transition temperature. Journal of Non-Crystalline Solids. 2015;428:68-74.

21.   Ediger MD, Harrowell P, Yu L. Crystal growth kinetics exhibit a fragility-dependent decoupling from viscosity. The Journal of Chemical Physics. 2008;128(3):034709.

22.   Kesterson MR. COMSOL Multiphysics Model for HLW Canister Filling. Aiken, SC: Savannah River National Laboratory; 2016. Contract No.: SRNL-STI-2015-00207.

23.   International A. Standard Test Methods for Determining Chemical Durability of Nuclear, Hazardous, and Mixed Waste Glasses and Multiphase Glass Ceramics: The Product Consistency Test (PCT). West Conshohocken, PA2014.

24.   Marcial J, Kabel J, Saleh M, Washton N, Shaharyar Y, Goel A, et al. Structural dependence of crystallization in glasses along the nepheline (NaAlSiO4) - eucryptite (LiAlSiO4) join. Journal of the American Ceramic Society. 2018;101(7):2840-55.

25.   Kroll J, Vienna J, Schweiger M. Effects of Al2O3, B2O3, Li2O, Na2O, and SiO2 on Nepheline Crystallization in Hanford High Level Waste Glasses: Ceramic Transactions, Volume CCLX. 2016. p. 159-69.

26.   Jantzen CM, Edwards TB. Defense Waste Processing Facility (DWPF) Viscosity Model: Revisions for Processing High TiO2 Containing Glasses. ; Savannah River Site (SRS), Aiken, SC (United States). Savannah River National Lab. (SRNL); 2016. Report No.: SRNL-STI-2016-00115; TRN: US1601913 United States 10.2172/1323882 TRN: US1601913 SRS English Contract No.: SRNL-STI-2016-00115.

27.   Mysen BO, Virgo D. Structure and Properties of Silicate Glasses and Melts; Theories and Experiment. Marfunin AS, editor. Berlin, Heidelberg: Springer Berlin Heidelberg; 1994.

28.   Zwanzig R. On the relation between self-diffusion and viscosity of liquids. The Journal of Chemical Physics. 1983;79(9):4507-8.

29.   Shelby J. Introduction to Glass Science and Technology: The Royal Society of Chemistry; 2005.

30.   Vienna JD, Crum JV. Non-linear effects of alumina concentration on Product Consistency Test response of waste glasses. Journal of Nuclear Materials. 2018;511:396-405.

31.   Lambotte G, Chartrand P. Thermodynamic modeling of the (Al2O3+Na2O), (Al2O3+Na2O+SiO2), and (Al2O3+Na2O+AlF3+NaF) systems. The Journal of Chemical Thermodynamics. 2013;57:306-34.

32.   Abdullaev GK, Rza-Zade PF, Mamedov KS. The system Na2O-Al2O3-B2O3. Zhurnal Neorganicheskoj Khimii. 1983;28(1):208-11.
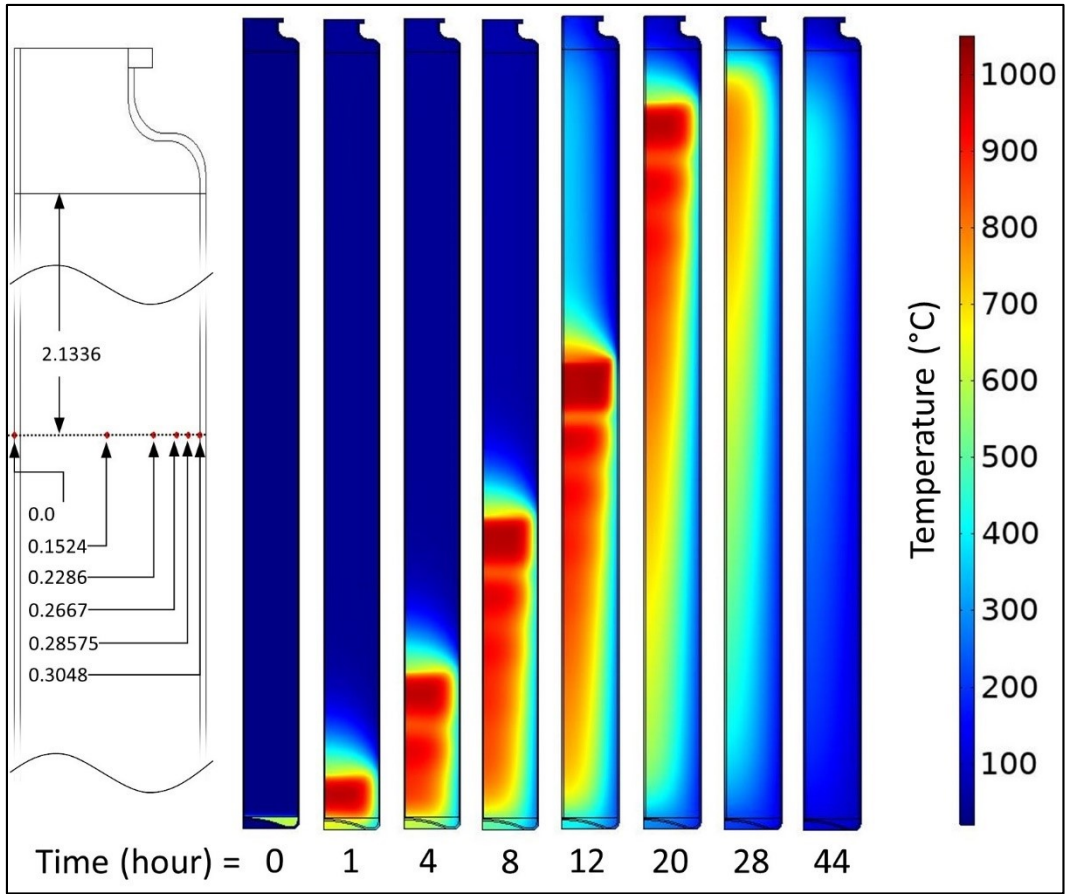
Figure 1: COMSOL® Multiphysics Modeling of a WTP HLW Canister Showing Glass Temperature During and After Pouring as a Function of Time and Location (Dimensions Shown in Meters)
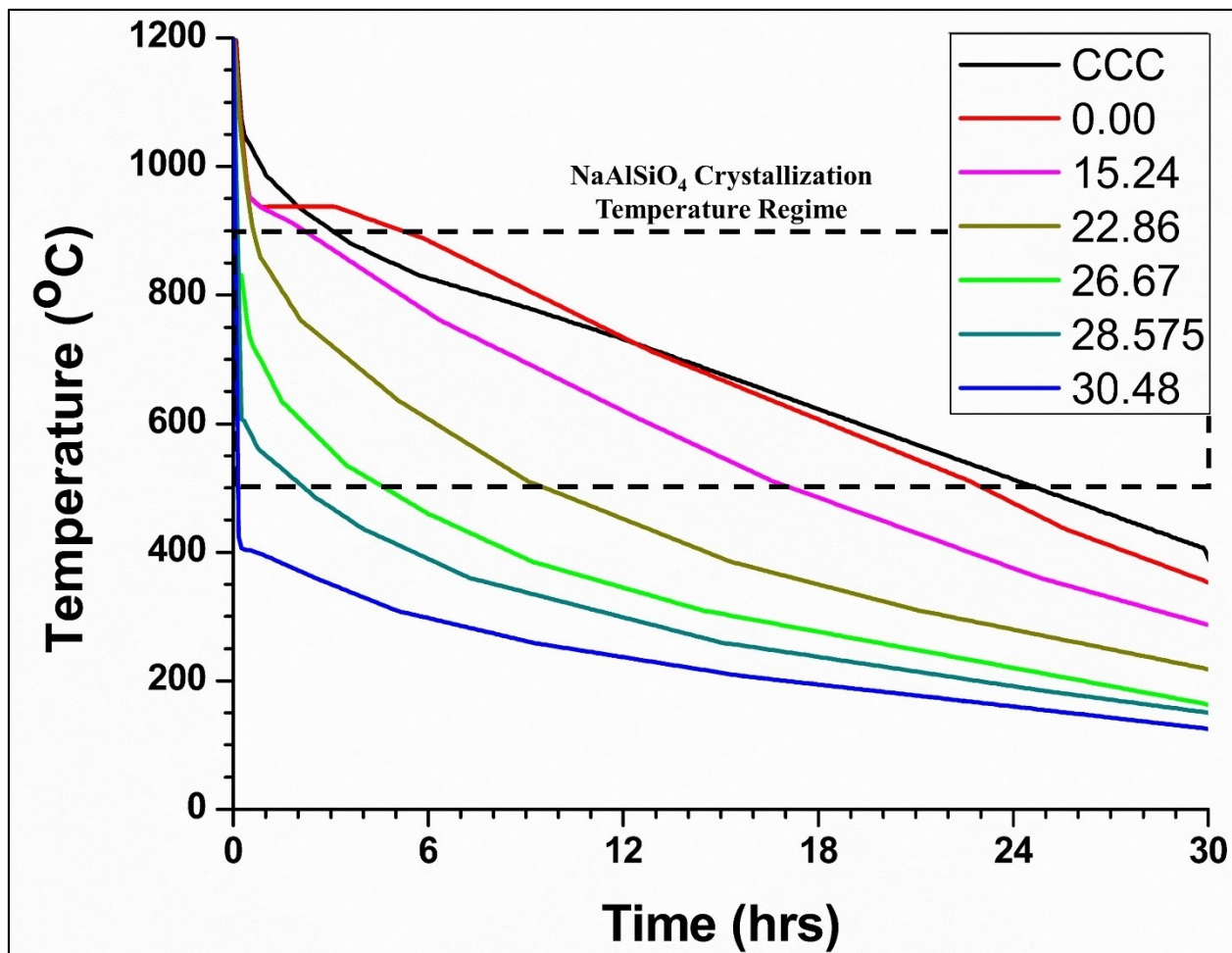
**Figure 2**: Cooling Profiles of Heat-Treated Specimens
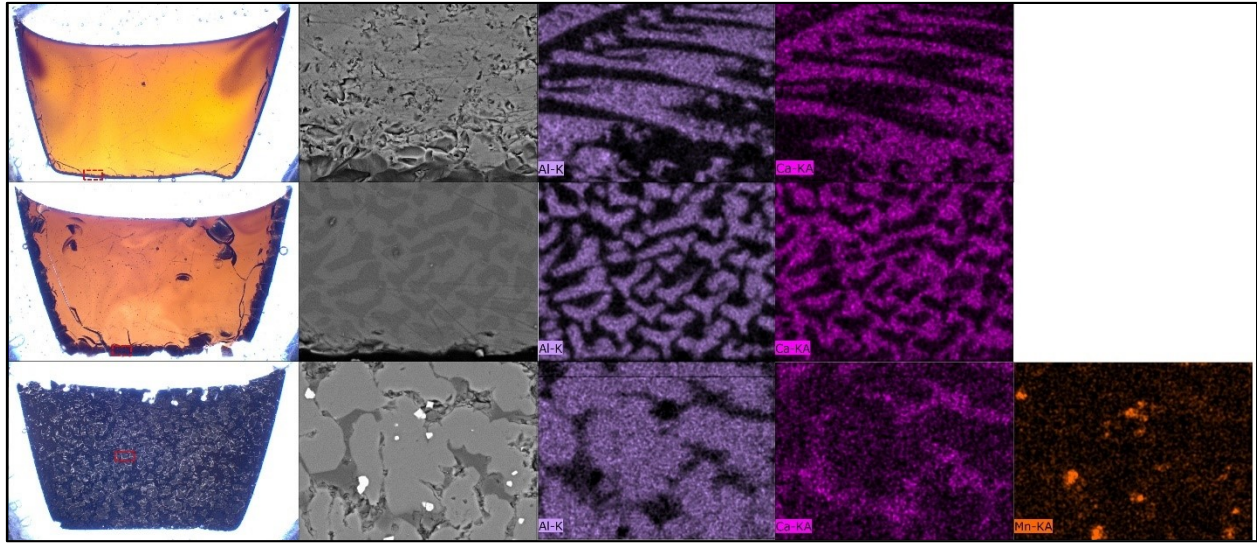
Figure 3: Optical and SEM/EDS images of NP2-23_15.24 (top), NP2-23_High Al_22.86 (center), and NP-MC-BNa-1_26.67(bottom). Red Boxes Show Approximate Location of SEM/EDS Images.
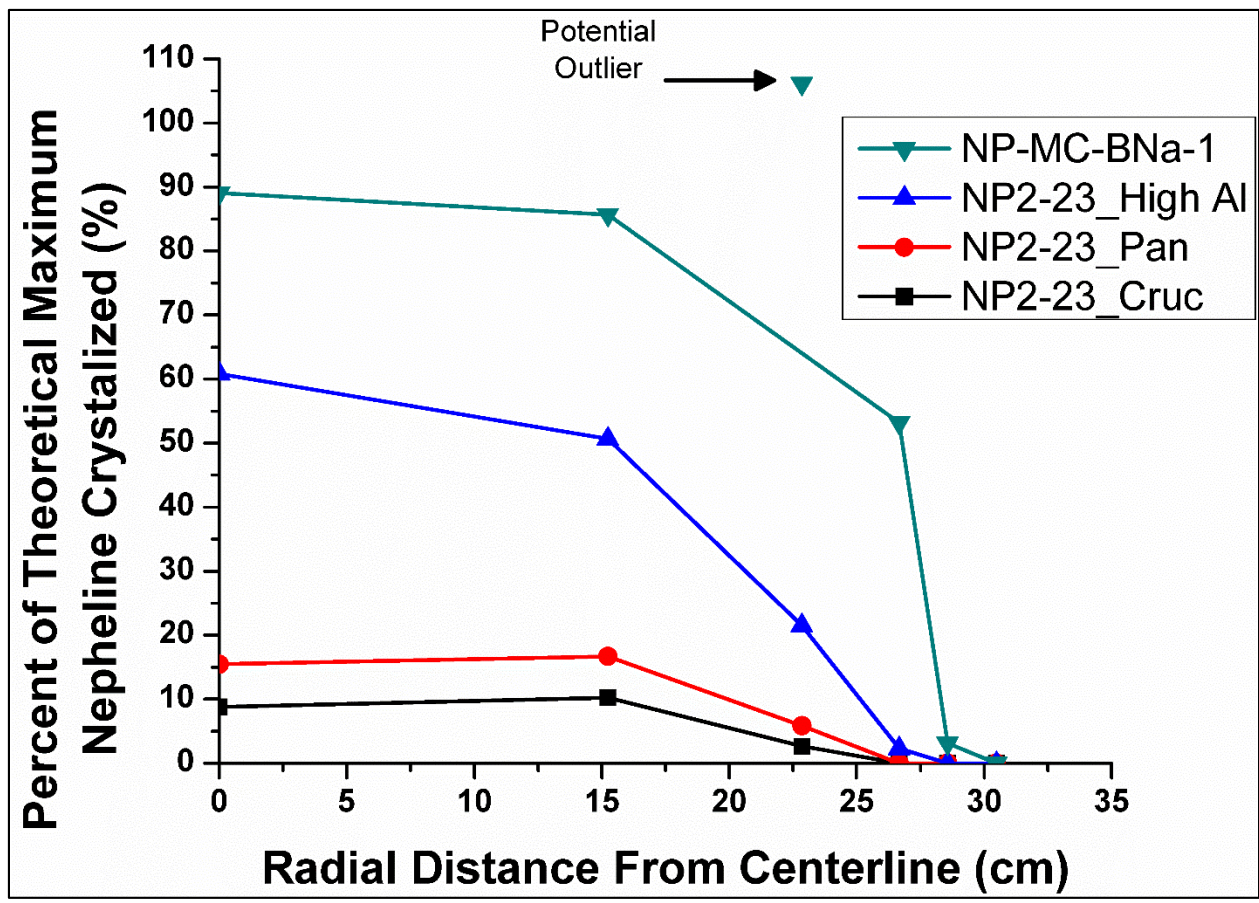
**Figure 4: Nepheline Crystallization as a Function of Canister Location Heat Treatment**
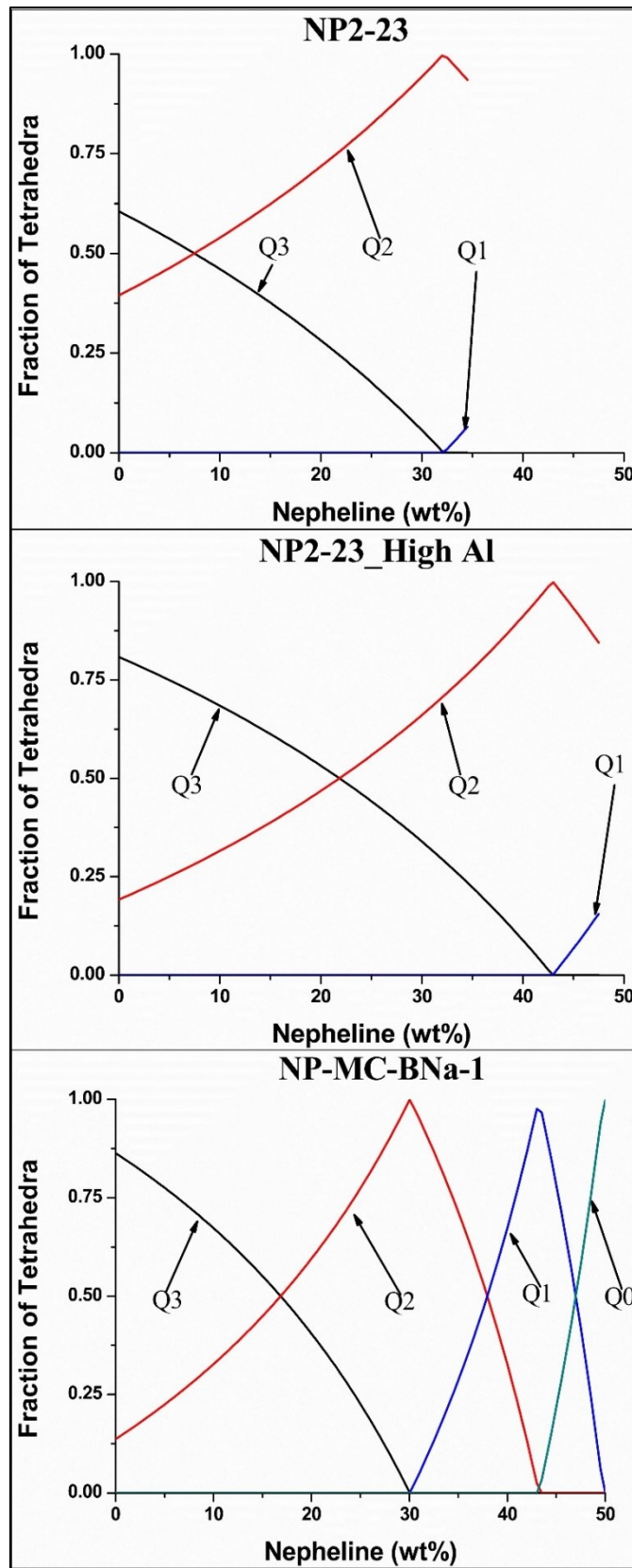
Figure 5: Calculated Q Units in Residual Glass
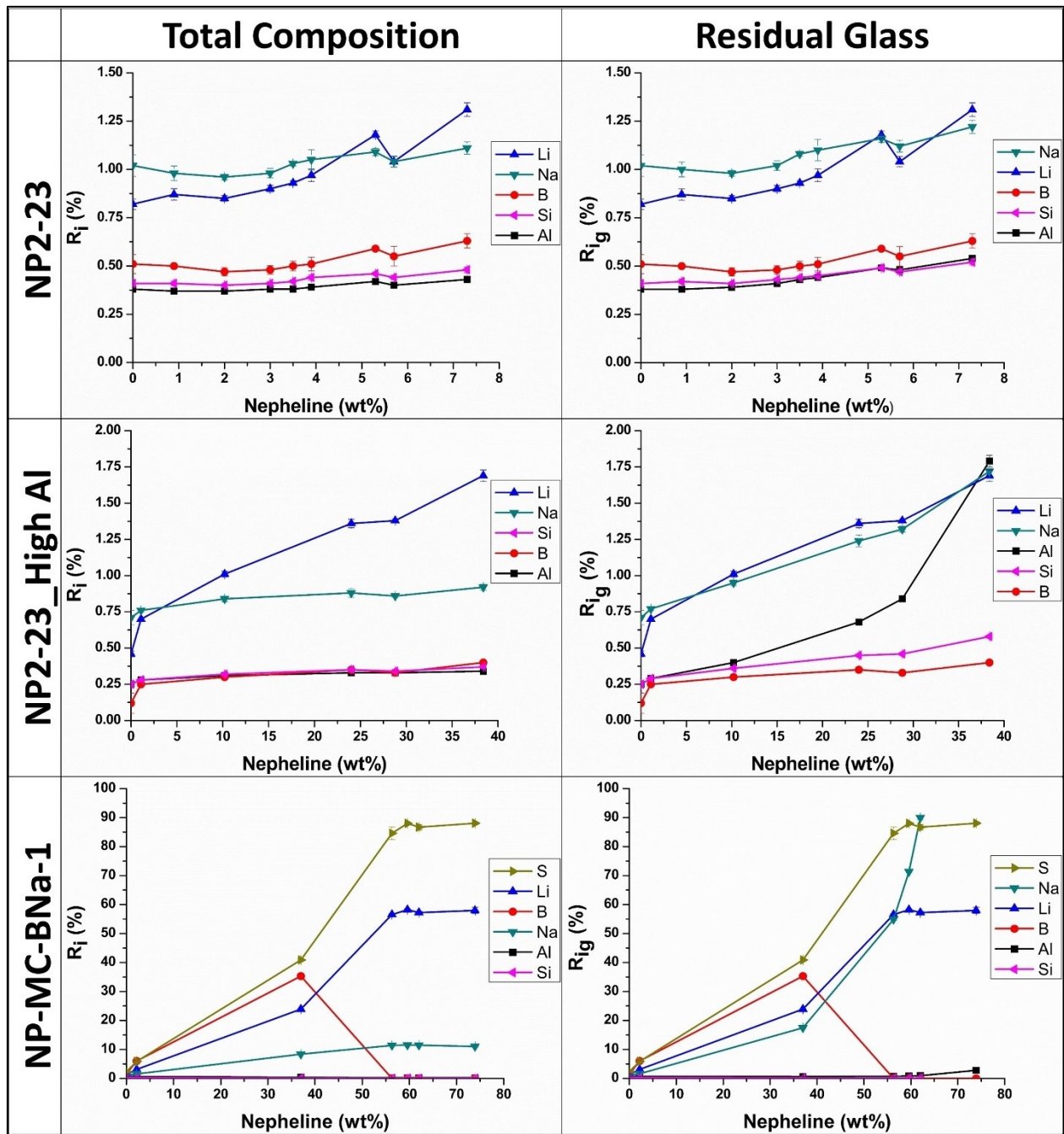
Figure 6: Normalized Release Relative to Total (left) and Residual (right) Glass Compositions
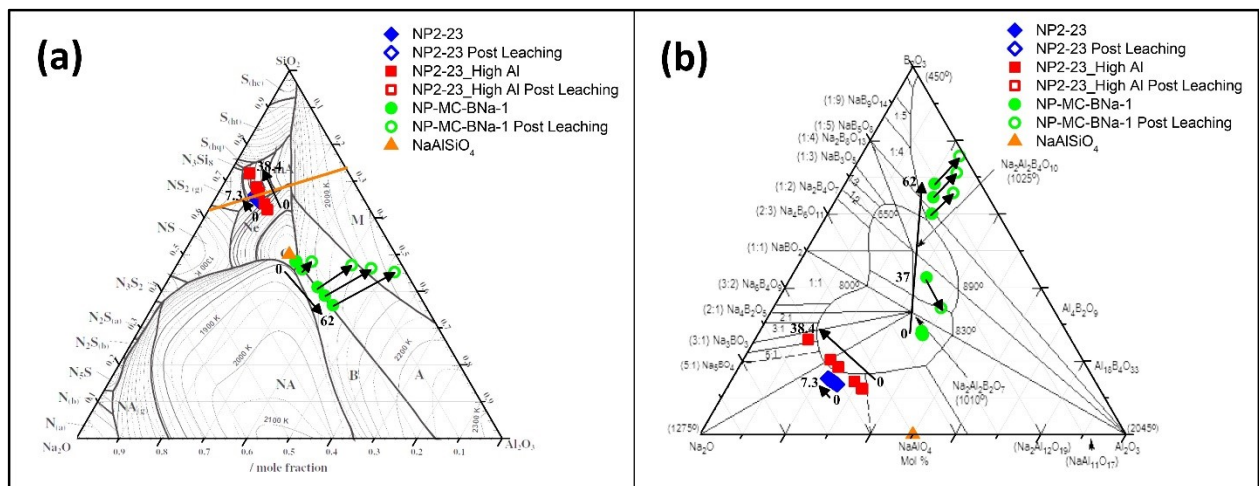
Figure 7: Glass Compositions Overlain on Na₂O-Al₂O₃-SiO₂(31) (a) and Na₂O-Al₂O₃-B₂O₃(32) (b) Phase Diagrams. Solid Symbols Represent Residual Composition Post Crystallization with Crystallization Content Increasing in the Direction of the Arrow, with Quantified PXRD Results Shown Next to Arrows, and Open Symbols Represent Final Compositions Post Leaching. Note that Solid and Open Symbols Overlay for Glasses Exhibiting Congruent Dissolution.

Table 1: **Targeted and Measured Glass Compositions**[*]

	NP2-23		NP2-23 High Al		NP-MC-BNa-1	
	Target (wt%)	Measured (wt%)	Target (wt%)	Measured (wt%)	Target (wt%)	Measured (wt%)
Al_2O_3	**12.28**	**11.17**	**17.00**	**15.60**	28.58	25.46
B_2O_3	4.50	4.14	4.50	4.04	14.00	12.82
Bi_2O_3	-	<0.11	-	<0.11	0.65	0.76
CaO	4.00	4.20	4.00	4.22	0.65	0.57
Cr_2O_3	0.20	0.20	0.20	0.18	1.10	0.93
F	-	nm	-	nm	0.30	nm
Fe_2O_3	7.22	6.50	2.50	2.30	2.51	2.29
Li_2O	4.00	3.93	4.00	4.02	5.01	5.15
MgO	1.50	1.37	1.50	1.28	-	<0.17
MnO	1.19	1.03	1.19	1.00	1.00	0.86
Na_2O	18.00	17.22	18.00	17.25	15.50	14.72
NiO	0.17	0.16	0.17	0.15	-	<0.13
P_2O_5	-	<0.23	-	<0.23	0.70	0.51
RuO_2	-	<0.13	-	<0.13	0.05	0.43
SO_3	-	<0.12	-	<0.12	0.25	0.26
SiO_2	44.94	43.44	44.94	43.73	**29.43**	**27.87**
TiO_2	2.00	1.78	2.00	1.82	-	<0.17
ZrO_2	-	<0.14	-	<0.14	0.25	0.17
Total	100	95.14	100	95.59	99.98	92.80
Maximum Nepheline (wt%)	34.2	31.1	47.4	43.5	69.6	65.9

[*]"nm" indicates that no attempt was made to measure the component and a dash is equivalent to zero.

Table 2: Cooling Steps for Furnace Heat Treatment

	CCC(15)		0.00 cm from centerline		15.24 cm from centerline		22.86 cm from centerline		26.67 cm from centerline		28.575 cm from centerline		30.48 cm from centerline	
	Rate (K/hr)	Finish Temperature (°C)	Rate (K/hr)	Finish Temperature (°C)	Rate (K/hr)	Finish Temperature (°C)	Rate (K/hr)	Finish Temperature (°C)	Rate (K/hr)	Finish Temperature (°C)	Rate (K/hr)	Finish Temperature (°C)	Rate (K/hr)	Finish Temperature (°C)
Step 1	750.0	1050	999.9	950	999.9	950	999.9	950	Moved to 825°C furnace		Moved to 600°C furnace		Moved to 400°C furnace	
Step 2	93.3	980	50.0	925	50.0	925	200.0	850	400.0	725	100.0	550	22.2	350
Step 3	48.4	930	2.3-hour dwell		25.0	900	80.0	750	100.0	625	42.9	475	20.0	300
Step 4	35.5	875	18.2	875	33.3	750	41.7	625	50.0	525	33.3	425	11.8	250
Step 5	23.3	825	25.0	700	25.0	600	31.3	500	30.0	450	23.1	350	8.0	200
Step 6	15.2	775	20.5	500	23.5	500	20.0	375	23.1	375	12.9	250	5.6	25
Step 7	16.7	725	25.0	425	18.2	350	13.0	300	14.3	300	7.5	175	-	
Step 8	18.2	400	18.6	25	14.0	25	10.2	25	9.3	25	6.5	25		

Table 3: **Measured Nepheline Concentration (wt%) from Quantitative XRD Analysis and Calculated Non-Bridging Oxygen (NBO) of Residual Glass**

	NP2-23_Crucible		NP2-23_Pan		NP2-23_High Al		NP-MC-BNa-1	
	Nepheline (wt%)	NBO	Nepheline (wt%)	NBO	Nepheline (wt%)	NBO	Nepheline (wt%)	NBO
Quenched	0.0	1.39	0.0	1.39	0.0	1.19	0.0	1.14
30.48	0.0	1.39	0.0	1.39	0.0	1.19	0.0	1.14
28.575	0.0	1.39	0.0	1.39	0.0	1.19	2.2	1.17
26.67	0.0	1.39	0.0	1.39	1.1	1.20	37.0	2.43
22.86	0.9	1.41	2.0	1.42	10.2	1.32	73.9	∞
15.24	3.5	1.44	5.7	1.47	24.0	1.54	59.6	7.93
0.00	3.0	1.44	5.3	1.47	28.8	1.63	62.0	10.44
CCC	3.9	1.45	7.3	1.50	38.4	1.87	56.3	5.96
Maximum Nepheline		2.06		2.06		2.15		∞